Image Segmentation for the Application of the Neugebauer Colour Prediction Model on Inkjet Printed Ceramic Tiles

P. Latorre[1], G. Peris-Fajarnes[1], and M.A.T. Figueiredo[2]

[1] Depto Exp Grafica en la Ingenieria, Universidad Politecnica Valencia
Ctra. Nazaret-Oliva s.n., 46730, Grao de Gandia, Valencia, Spain
{platorre, gperis}@degi.upv.es
[2] Instituto de Telecomunicaçoes, Instituto Superior Tecnico
Torre Norte, Piso 10, Av. Rovisco Pais, 1049-001, Lisboa, Portugal
mtf@lx.it.pt

Abstract. Colour prediction models (CPM) can be used to analyze the printing quality of halftone-based color printing systems. In this paper, we consider the Neugebauer CPM which requires as input the fraction of occupation of each primary. To obtain these numbers, we apply several image segmentation algorithms, with and without contextual information. These segmentation algorithms are evaluated with respect to another technique based on mixtures of factor analyzers. More importantly, the segmentation results are evaluated with respect to the performance of the Neugebauer CPM when used with the obtained fractions of occupation. This evaluation is carried out by comparing the predicted color against that measured with a spectrophotometer, and testifies for the adequacy of the approach.

1 Introduction

The macroscopic color of a halftone design depends on several factors, including the morphology, ink distribution, and occupation area of the printed dots. Several approaches allow relating the microscopic distribution of dots with the resulting average macroscopic color [12]. These approaches, which are important in practice since they allow controlling the printing process, can be divided into two classes:

Regression-based: Some regression curve is adjusted to experimental data (usually in a minimum mean squared error sense), without considering the physics of the printing process. There are several regression-based models, such as Neugebauer, Murray-Davies, Yule-Nielsen, modified Neugebauer, and others [12].

From "first principles": These approaches are based on physical models of the processes occurring during and after printing; they are harder to implement and, as far as we know, haven't achieved the performance of regression-based methods [12].

In this paper we apply the *Neugebauer color prediction model* (N-CPM) to printed ceramic tiles. The N-CPM requires as input the relative area coverage of each printing primary. To obtain estimates of these numbers, we apply several non-contextual and

M. Kamel and A. Campilho (Eds.): ICIAR 2005, LNCS 3656, pp. 9–16, 2005.

contextual segmentation algorithms to the microscopic images of the printed surfaces. All algorithms are tested on two color spaces: RGB and the so-called *opponent color space* (OCS) [13], which were previously shown to give good results with one kind of printed dot [6]. As far as we know, CPMs have only recently been applied to ceramic tiles, but not using image analysis methods [4].

Section 2 describes the N-CPM and the experimental methods used to obtain the printed ceramic tiles and the corresponding images. In Section 3, we briefly discuss color image smoothing and the segmentation algorithms. Section 4 describes the generation of "ground-truth" images based on mixtures of factors analyzers [3]. Experimental results are reported in Section 5. The paper is concluded in Section 6.

2 The Neugebauer Color Prediction Model and the Experimental Procedure

We consider halftone designs of two inks, printed with an industrial binary CMYK inkjet printer for ceramic tiles [5]. For this type of printer, there are 2^4 basic colors, called Neugebauer primaries [12]: the single colors cyan (C), magenta (M), yellow (Y), and black (K); all binary overlaps (CM, CY, MY, CK, MK, YK); all ternary overlaps (CMY, CMK, CYK, MYK), the single full overlap (CMYK), and the background.

According to the spectral Neugebauer CPM (N-CPM) [12], the overall reflectance of a halftone pattern is predicted as

$$R(\lambda) = \sum_i a_i R_i(\lambda), \tag{1}$$

where λ denotes wavelength, $R_i(\lambda)$ is the spectral reflectance curve (as a function of wavelength) of the i^{th} Neugebauer primary at full colorant coverage, and a_i is the fractional relative area coverage of that printing primary (with $\sum_i a_i = 1$).

To assess the N-CPM for two kinds of dots, we digitally created and printed two rows of $3 \times 3\ cm^2$ halftones with the two inks, one of them with a theoretical dot area percentage fixed at 20%, and the other increasing from 20% to 80% in 10% steps (see Fig. 1, Left) on $20cm \times 30cm$ tiles with engobe and matt glaze layers on a fired biscuit base (for better consistency). Each square is named with the corresponding colors and dot area percentages; *e.g.*, C20M30 refers to 20% cyan and 30% of magenta (theoretical). We also created $3 \times 3\ cm^2$ color squares with 100% occupation of the corresponding Neugebauer primaries for these halftones; *e.g.*, for cyan and magenta, these would be cyan, magenta, and overlapping, at 100% occupation, as well as background.

We acquired images using a CCD color camera with a zoom lens, under a bank of two 36-Watt daylight fluorescent lamps. The imaged area was $7mm \times 8.5mm$, at $50cm$ distance from the base of the camera to the tile surface (see Fig. 1).

For the application of the N-CPM, we measured reflectance curves of a $8mm$ radius circle of each halftone square patch, as well as of each Neugebauer primary with an *integrating sphere MINOLTA CM-508i spectrophotometer*, with illumination-geometry $D65/10^\circ$. The spectral range covered is $[400 - 700]\ nm$, in $10nm$ steps.

The segmentation algorithms will provide estimates of the a_i parameters for use in (1). This allows comparing the N-CPM predicted reflectance curve with the corresponding spectrophotometer curve to assess its validity.

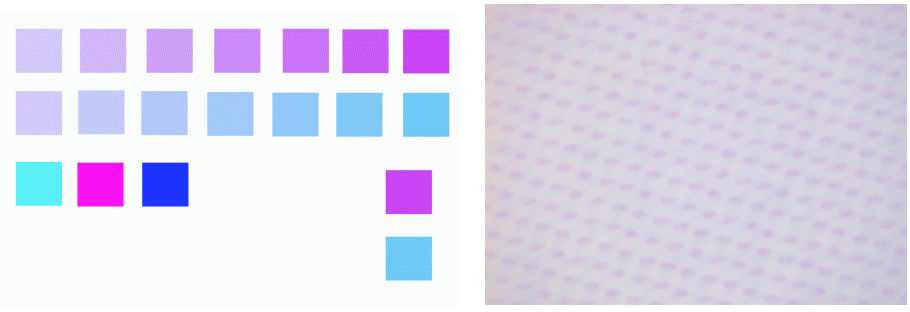

Fig. 1. Left: Digitally created file for C and M. First row, Cyan fixed at 20%. Second row, Magenta fixed at 20%. Right: Image of C at 30% and M at 20% acquired with the Zoom lens.

3 Segmentation Algorithms to Estimate Dot Area

Due to the noise in the acquired images, they are pre-processed by a non-linear, edge-preserving, multichannel smoothing filter called *adaptive nearest neighbor filter*, the details of which are found in [6] and [2]. To segment the images, we used the following techniques, both in RGB and OCS: fuzzy C-means (FCM); FCM with contextual information based on a Markov random field (FCM-MRF) [11]; mixture of Gaussians (MoG); contextual MoG, via the iterated conditional modes (ICM) algorithm [7], [8]; a new MoG method which also smoothes the posterior class probability estimates. For a detailed description of the FCM and FCM-MRF approaches, we refer the reader to [11].

The MoG model for images with two types of dots (say, cyan and magenta) considers each pixel as a sample of a random variable in $I\!R^3$ (RGB or OCS) with a 4-component MoG probability density function,

$$p(y) = \sum_{j=1}^{4} a_j \, \mathcal{N}(y|\mu_j, C_j);$$

the four Gaussian components correspond to the four Neugebauer primaries: pure cyan, pure magenta, overlap, and background. Parameters μ_j and C_j are the mean vector and covariance matrix of each component, while a_j is the weight of component j, to be used in the N-CPM equation (1). The standard expectation-maximization (EM) algorithm [7] obtains estimates of these parameters from a set of samples (pixels) $\{y_i, i = 1, ..., N\}$ by iterating two steps:

E-step: Compute the *a posteriori* probability that pixel i, for $i = 1, ..., N$, was produced by component j (given the current estimates $\widehat{a}_j$, $\widehat{\mu}_j$, and $\widehat{C}_j$)

$$\tau_{ij} = \frac{\widehat{a}_j \, \mathcal{N}(y_i|\widehat{\mu}_j, \widehat{C}_j)}{\sum_{k=1}^{4} \widehat{a}_k \, \mathcal{N}(y_i|\widehat{\mu}_k, \widehat{C}_k)}, \qquad \text{for } \; j = 1, 2, 3, 4; \tag{2}$$

M-step: Update the parameter estimates according to (for $j = 1, 2, 3, 4$)

$$\widehat{a}_j = \frac{\sum_i \tau_{ij}}{N}, \qquad \widehat{\mu}_j = \frac{\sum_i y_i \, \tau_{ij}}{\sum_i \tau_{ij}}, \qquad \widehat{C}_j = \frac{\sum_i (y_i - \widehat{\mu}_j)(y_i - \widehat{\mu}_j)^T \, \tau_{ij}}{\sum_i \tau_{ij}}.$$

The ICM approach is based on the same MoG model. The first phase of this approach is to run the EM algorithm until convergence. In the second phase, a modified EM algorithm is applied, based on a modified E-step in which the *a posteriori* probabilities are spatially smoothed using a window centered on that pixel:

$$\tau'_{ij} = \frac{\eta_{ij}\, \mathcal{N}(y_i|\widehat{\mu}_j, \widehat{C}_j)}{\sum_{k=1}^{4} \eta_{ik} \mathcal{N}(y_i|\widehat{\mu}_k, \widehat{C}_k)}, \qquad \text{with} \qquad \eta_{ij} = \frac{\exp(\beta \sum_{n\in W_i} \tau_{nj})}{\sum_{k=1}^{4} \exp(\beta \sum_{n\in W_i} \tau_{nj})}, \quad (3)$$

where W_i is a window centered around pixel i and the τ_{ij} are computed according to the standard E-step (2). The smoothed τ'_{ij} posterior probabilities are then used in the standard M-step.

We also propose a new method to smooth the *a posteriori* probabilities. The key idea is that each set of *a posteriori* probabilities $\{\tau_{i1}, ..., \tau_{i4}\}$, which have to be nonnegative ($\tau_{ij} \geq 0$) and normalized ($\tau_{i1} + ... + \tau_{i4} = 1$), can be expressed by 3 unconstrained real variables $\{\alpha_{i1}, \alpha_{i2}, \alpha_{i3}\}$ using a so-called multinomial logistic transformation:

$$\tau_{i1} = \frac{e^{\alpha_{i1}}}{1 + \sum_{j=1}^{3} e^{\alpha_{ij}}}, \quad \tau_{i2} = \frac{e^{\alpha_{i2}}}{1 + \sum_{j=1}^{3} e^{\alpha_{ij}}}, \quad \tau_{i3} = \frac{e^{\alpha_{i3}}}{1 + \sum_{j=1}^{3} e^{\alpha_{ij}}}, \quad \tau_{i4} = \frac{1}{1 + \sum_{j=1}^{3} e^{\alpha_{ij}}}. \quad (4)$$

This transformation is of course invertible according to

$$\alpha_{i1} = \log\left(\frac{\tau_{i1}}{\tau_{i4}}\right), \quad \alpha_{i2} = \log\left(\frac{\tau_{i2}}{\tau_{i4}}\right), \quad \alpha_{i3} = \log\left(\frac{\tau_{i3}}{\tau_{i4}}\right). \quad (5)$$

The proposed approach consists of computing the α_{ij} variables according to (5) after the last E-step, spatially smoothing these variables using any filter (since these variables are under no constraints) and then recomputing the τ_{ij} variables using (4).

4 Obtaining the "Groundtruth" Segmentations

In [6] it was shown, for one type of printed dot, that singular value decomposition (SVD) could be used to create images that can be seen as *groundtruth*. In fact, the SVD was just the first of a series of steps which included morphological operations and the *connected components labelling* method; see [6] for full details. For images of two printed dots, we propose the use of mixtures of factors analyzers (MFA) [3], which can be seen as a local generalization of factor analysis (FA, [1]). For lack of space, we can not give details of the MFA approach, and the reader is referred to [3] for more information. Fig. 2 shows examples of these segmentations obtained by MFA, after some post-processing steps [6], as well as segmentations obtained by the ICM algorithm described in Section 3.

5 Results and Discussion

5.1 Segmentation Results

To compare the segmentation results produced by the algorithms described in Section 3 with the MFA-based segmentations, we computed sensitivity *per class* (SC)

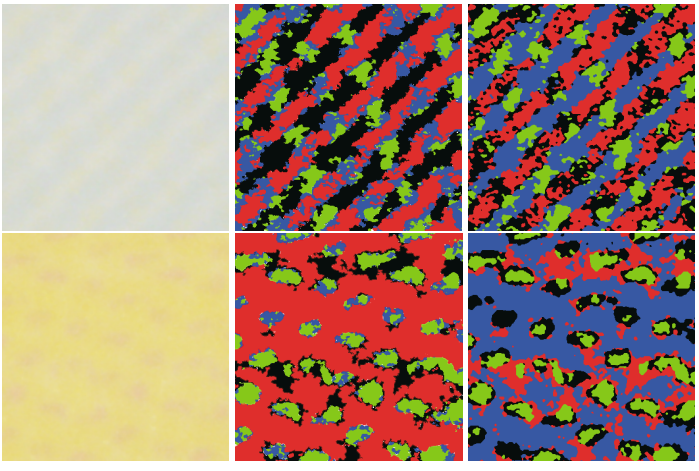

Fig. 2. Left column: original images of $C50Y20$ and $M20Y80$. Center column: corresponding MFA-generated *groundtruth*. Right column: ICM based segmentation results.

Table 1. Sensitivities (per class) and overall accuracies. $GS1$ means Gaussian smoothing with standard deviation $\sigma = 0.3$ with a $3 \cdot 3$ window size. $GS2$, standard deviation $\sigma = 1.0$ with a $3 \cdot 3$ window size. $GS3$, standard deviation $\sigma = 1.0$ with a $5 \cdot 5$ window size. $GS4$, standard deviation $\sigma = 3.0$ with a $5 \cdot 5$ window size. ANN is the adaptation of the Adaptive Nearest Neighbour Filter, as in [2], applied on a $3 \cdot 3$ window.

	SC-C	SC-M	SC-Y	SC-CM	SC-CY	SC-MY	SC-Back	Overall accuracy
FCM	67,23	67,41	69,37	61,66	54,75	66,64	75,81	64,46
FCM-MRF	67,53	65,61	69,77	62,24	56,43	66,87	75,72	64,75
EM	67,54	74,70	71,62	70,26	57,42	82,60	81,20	73,64
EM - ICM	68,17	**75,72**	**72,32**	70,90	**58,34**	82,18	**82,31**	**74,08**
EM GS1	67,86	74,58	72,28	70,75	57,83	83,04	81,23	74,02
EM GS2	67,99	74,29	72,07	70,67	57,84	82,95	81,15	73,94
EM GS3	68,15	74,07	71,93	70,87	58,07	83,07	81,03	73,90
EM GS4	68,23	73,69	71,55	71,02	58,24	83,05	80,74	73,73
EM ANN	67,53	74,52	71,95	70,22	57,90	82,39	81,07	73,79

values as well as overall accuracies (OA). These quantities are given by: $SC = TP/(TP + FN)$, where TP stands for "true positives" and FN for "false negatives"; $OA = NCC/(NCC + NIC)$, where NCC denotes the "number of correct classifications" and NIC means "number of incorrect classifications". Table 1 reports results for all segmentation methods in RGB (all methods did worse in OCS, so we omit those results). We see that the ICM algorithm gives the best results in terms of OA. The alternative method that we have proposed performs only slightly worse, with the advantage that the contextual part is applied only once.

5.2 Assessing the Neugebauer Model

We assess the N-CPM by comparing the experimentally measured spectral reflectance for each printed patch (see Section 2) against the spectral curves predicted by the N-

Table 2. Comparing spectrophotometer and model predicted reflectance curves: first row in each case is the MFA-based result, the second row is the result by the ICM algorithm

	RMS value (%)	DeltaE76	DeltaE00	MI00
C20M20	6,74	4,86	3,66	1,99
	5,31	3,27	2,30	1,36
C20M30	8,15	5,50	3,98	1,74
	4,69	2,93	2,39	1,48
C20M40	8,75	6,90	5,09	1,70
	6,81	4,84	4,02	2,07
C20M50	7,73	4,98	3,80	1,63
	5,82	5,25	4,53	1,89
C20M60	5,12	3,97	3,07	1,24
	5,98	4,22	3,27	1,38
C20M70	3,69	6,25	4,37	0,44
	4,79	6,86	4,99	1,28
C20Y20	2,25	1,34	1,00	0,53
	5,56	3,58	2,58	1,16
C20Y30	7,77	7,66	5,71	2,33
	4,37	3,54	2,54	1,31
C20Y40	6,20	3,98	2,68	1,72
	5,52	5,63	3,87	1,62
C20Y50	4,96	6,05	4,03	0,94
	3,97	3,14	2,02	1,15
C20Y60	1,55	1,24	1,04	0,22
	1,87	1,13	1,11	0,15
C20Y70	6,57	10,25	6,00	1,05
	6,27	9,26	5,39	0,76
M20Y20	4,30	2,89	2,14	0,72
	4,83	3,76	2,68	0,67
M20Y30	6,40	5,03	3,43	0,78
	5,05	3,75	2,64	0,76
M20Y40	8,40	7,30	6,91	1,02
	8,76	7,50	6,99	1,03
M20Y50	5,48	5,01	3,07	0,77
	8,89	7,69	7,06	1,06
M20Y60	4,95	3,88	2,66	0,79
	4,76	5,86	5,13	0,91
M20Y70	5,47	5,99	4,95	0,89
	3,95	4,39	3,39	0,80

CPM based on the *groundtruth* segmentation and the one obtained by the ICM algorithm described in Section 3. The predicted spectral curves are obtained by plugging the estimated dot area coverage (parameters a_i from the segmentations) and the reflectance curves of the Neugebauer primaries into (1). To compare predicted and mea-

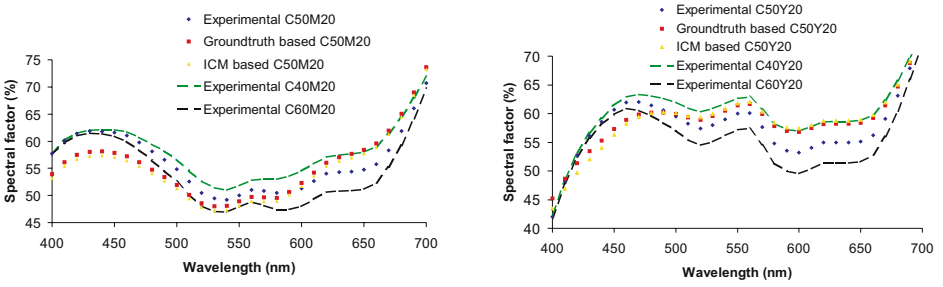

Fig. 3. Model predicted spectral reflectance curves of $C50M20$ and $C50Y20$

sured spectral reflectance curves, we use the following quantities [10]: the root mean squared (RMS) error between the two curves; the $\Delta E_{L^*a^*b^*}$ color difference; the ΔE_{00} color difference; and the metameric index MI_{00}. The $\Delta E_{L^*a^*b^*}$ and ΔE_{00} colour differences are particularly relevant since they try to match the human color perception. The procedure to obtain an $L^*a^*b^*$ color from a spectral reflectance curve is described in [6].

Table 2 shows values for a set of test images. It is known that humans can only discern color differences when $\Delta E_{L^*a^*b^*} > 3.5$ [9]. Thus, we can state that the MFA-based results and the results produced by the ICM algorithm yield good colour predictions with the Neugebauer model.

In Fig. 3 we can see the experimental and predicted reflectance curves for two cases: $C50Y20$ and $C50M20$. For $C50Y20$, we also show $C40Y20$ and $C60Y20$ reflectance curves, and for $C50M20$, we show the $C40M20$ and $C60M20$ curves. These curces can be seen as a kind of bounds for the predicted reflectances. These two plots show a slight limitation in the lower part of the spectrum, for these two cases, of the prediction capability.

6 Conclusion

We have investigated the use of some non-contextual and contextual segmentation algorithms for images of halftone patterns with two types of printed dots, taken from ink-jet printed ceramic surfaces. *Groundtruth* and ICM segmentation results are used to feed a Neugebauer colour prediction model which outputs predictions of spectral reflectance curves. These predicted curves were compared with experimental ones (obtained with a spectrophotometer) under several error measures (some of them of perceptual nature). We have concluded that the predicted colors are close to the measured ones.

This paper has established a color prediction framework for ink-jet printing technology on ceramic tiles for four-color patterns. The next step will be to analyze images with three types of printed dots (C, M and Y), which implies the existence of 8 (2^3) different clusters, four of which correspond to overlapping of inks.

Acknowledgements

This work has been partially funded by the European Project MONOTONE (G1RD-CT-2002-00783).

References

1. A. Basilevsky, *Statistical Factor Analysis and Related Methods.* John Wiley & Sons New York (1994).
2. M. J. Cree, "Observations on Adaptive Vector Filters for Noise Reduction in Color Images," *IEEE Signal Processing Letters,* vol. 11, no. 2 (2004) 140-143.
3. Z. Ghahramani, G. Hinton, *The EM algorithm for Mixtures of Factor Analyzers.* Technical Report CRG-TR-96-1 University of Toronto (1996).
4. L. Iovine, S. Westland, T. L. V. Cheung, "Application of Neugebauer-based Models to Ceramic Printing," *IS&T / SID Twelfth Color Imaging* (2004) 176-180.
5. Kerajet Ink-Jet printing system. http://www.kerajet.com
6. P. Latorre, G. Peris-Fajarnes, M. Mirmehdi, B. Thomas, "Assessing the Neuegbauer Colour Prediction Model for Ink-jet Printed Ceramic Tiles," *Proceedings of the 4th IASTED International Conference on Visualization, Imaging, and Image Processing,* (2004) 636-641.
7. G. McLachlan, D. Peel, *Finite Mixture Models,* John Wiley & Sons New York (2000).
8. G. McLachlan, S. K. Ng, G. Galloway, D. Wang, "Clustering of Magnetic Resonance Images," *Proceedings of the American Statistical Association (Statistical Computing Section).* (1996) 12-17.
9. M. Stokes, M. D. Fairchild, R. S. Berns, "Colorimetrically Quantified Visual Tolerances for Pictorial Images," *Proceedings of TAGA,* (1992) 757-778.
10. L. A. Taplin, R. S. Berns, "Spectral Color Reproduction Based on Six-color Inkjet Output System," *Proceedings of the Ninth Color Imaging Conference: Colour Science and Engineering, Systems, Technologies, and Applications,* Springfield (2000) 209-213.
11. R. Wiemker, "Unsupervised Fuzzy Classification of Multispectral Imagery Using Spatial-Spectral Features," *Proceedings of the 21st Annual Meeting of the Gessellschaft für Klassifikation – GfKI'97,* pp. 12-14, Postdam, 1997.
12. D. Wyble, "A Critical Review of Spectral Models applied to Binary Color Printing," *Color Research and Applications*, vol. 25, (2000) 4-19.
13. X. Zhang, B. A. Wandell, "A Spatial Extension of Cielab for Digital Color Image Reproduction," *Society for Information Display* (1996).